

Luteolin-Loaded Nanoparticles for the Treatment of Melanoma

Qiao-Ting Fu^{1,*}, Xiao-Qin Zhong^{1,*}, Mei-Yu Chen^{1,*}, Jia-Yi Gu², Jian Zhao³, De-Hong Yu⁴, Fei Tan^{1,5}

¹Shanghai Skin Disease Clinical College, The Fifth Clinical Medical College, Anhui Medical University, Shanghai Skin Disease Hospital, Shanghai, 200443, People's Republic of China; ²Department of Otolaryngology-Head and Neck Surgery, Shanghai Ninth People's Hospital, Shanghai Jiao Tong University, School of Medicine, Shanghai, 200011, People's Republic of China; ³Department of Oncology-Pathology, Karolinska Institutet, BioClinicum, Karolinska University Hospital Solna, Solna, Sweden; ⁴Materdine Lab, School of Life Sciences, Shanghai University, Shanghai, 200444, People's Republic of China; ⁵Shanghai Skin Disease Hospital, School of Medicine, Tongji University, Shanghai, 200443, People's Republic of China

*These authors contributed equally to this work

Correspondence: Fei Tan; Dehong Yu, Email tanfeitrue@126.com; dehongyu@126.com

Background and Purpose: Luteolin (LUT), a flavonoid found in various plants, has been reported to have potential therapeutic effects in melanoma. However, poor water solubility and low bioactivity have severely restricted the clinical application of LUT. Based on the high reactive oxygen species (ROS) levels in melanoma cells, we developed nanoparticles encapsulating LUT with the ROS-responsive material poly(propylene sulfide)-poly(ethylene glycol) (PPS-PEG) to enhance the water solubility of LUT, accelerate the release of LUT in melanoma cells, and further enhance its anti-melanoma effect, providing a viable solution for the application of LUT nano-delivery systems in melanoma therapy.

Methods: In this study, LUT-loaded nanoparticles were prepared with PPS-PEG and named as LUT-PPS-NPs. Dynamic light scattering (DLS) and transmission electron microscopy (TEM) were applied to determine the size and morphology of LUT-PPS-NPs. In vitro studies were carried out to determine the uptake and mechanism of LUT-PPS-NPs by SK-MEL-28 melanoma cells. According to the CCK-8 assay, the cytotoxic effects of LUT-PPS-NPs on human skin fibroblasts (HSF) and SK-MEL-28 cells were assessed. Apoptosis assays, cell migration and invasion assays, and proliferation inhibition assays with low and normal density plating were also applied to test the in vitro anti-melanoma effect. Additionally, melanoma models were established utilizing BALB/c nude mice and initially evaluated the growth inhibitory impact following intratumoral injection of LUT-PPS-NPs.

Results: The size of LUT-PPS-NPs was 169.77 ± 7.33 nm with high drug loading ($15.05 \pm 0.07\%$). In vitro, cellular assays confirmed that LUT-PPS-NPs were efficiently internalized by SK-MEL-28 cells and showed low cytotoxicity against HSF. Moreover, LUT released from LUT-PPS-NPs significantly inhibited tumor cell proliferation, migration and invasion. Animal experiments showed that LUT-PPS-NPs inhibited tumor growth more than 2-fold compared with the LUT group.

Conclusion: In conclusion, the LUT-PPS-NPs developed in our study enhanced the anti-melanoma effect of LUT.

Keywords: luteolin, melanoma, nanoparticles, PPS-PEG, drug delivery system

Introduction

Melanoma is a highly malignant tumor originating from melanocytes which is characterized by high multidrug resistance, a tendency to metastasize and relapse, and has the highest mortality rate of all skin cancers.¹ Treatment of melanoma includes local and systemic treatment, such as surgery, radiotherapy, chemotherapy, immunotherapy, molecular targeted therapy, and combination therapy.²⁻⁴ The available treatment modalities for advanced melanoma have considerable side effects and are prone to recurrence along with high treatment costs.⁵ Hence, more alternative treatment options are required. In recent years, an increasing number of natural plant-derived ingredients have been demonstrated to have therapeutic effects on various cancers.⁶

Luteolin (LUT, 3',4',5,7-tetrahydroxyflavone) is a natural flavonoid commonly found in a variety of fruits, vegetables, and herbs, and has a variety of biological activities such as anti-inflammatory, anti-allergic, antioxidant, and anti-cancer properties.^{7–10} Current studies have shown that LUT appears to be a promising plant extract with the potential for the prevention and treatment of melanoma.^{8,11,12} LUT can stimulate autophagy while inducing apoptosis in C32 human melanoma cells.¹³ It has been reported that LUT can inhibit the migration of A375 human malignant melanoma cells, induce apoptosis and reduce invasive potential.¹⁴ In other malignant melanoma cell lines (SK-MEL-2, SK-MEL-28 and WM3211 cells), LUT affected the proliferation and invasion of these cells by interfering with the extracellular matrix (ECM) pathway.¹⁵ In addition, its anti-tumor effect *in vivo* has been confirmed.^{11,14,16} Despite the promising potential of LUT in the prevention and treatment of melanoma, its clinical application is limited by poor water solubility and low oral bioavailability.^{17,18} Nano-drug delivery systems (NDDS) loaded with LUT may be an effective strategy to overcome these limitations.¹⁹

NDDS have unique advantages for improving the water solubility and bioavailability of insoluble drugs as well as enhancing therapeutic efficacy. Furthermore, NDDS have been widely studied in the past decades for targeted treatment of solid cancers.^{20–23} Nanoparticles (NPs) offer several benefits in the anti-tumor field, such as better drug storage stability, reduced dosing frequency and circumvention of multidrug resistance in tumor cells.²⁴ Drug-carrying NPs have been shown to prolong the circulation time of small molecule drugs and to passively target tumor sites due to their enhanced permeability and retention effect (EPR).²⁵

Reactive oxygen species (ROS) are closely related to the occurrence and development of cancer. ROS levels in tumor tissues have been reported to be thousands of times greater than in normal tissues, while cancer cells, especially melanoma cells, exhibit high amounts of ROS.^{26,27} Based on the abnormal microenvironment of tumor tissues, ROS-responsive materials have been extensively developed for cancer therapy. These efficient responsive drug delivery systems can intelligently release therapeutic drugs in the ROS microenvironment, improving therapeutic efficiency and reducing side effects.^{28–30} Poly(propylene sulfide)-poly(ethylene glycol) (PPS-PEG) is a common ROS-responsive material. The hydrophilic poly(ethylene glycol) (PEG) is resistant to protein adsorption and has low toxicity, while the hydrophobic poly(propylene sulfide) (PPS), a thioether-containing polymer, is key to the ROS-responsive of PPS-PEG, which can transition from the hydrophobic sulfide phase to the hydrophilic poly(propylene sulfoxide) and the ultimate poly(propylene sulfone) in an oxidizing environment.^{30–33} This property can be used to increase the water solubility of hydrophobic drugs. In applications, PPS-PEG is a widely used and easily synthesized material with properties such as oxidation-induced switch-like solubility changes and excellent biocompatibility. And it is reactive to ROS, including H₂O₂, leading to solubility changes that dissociate the nanocarrier and release the drug it encapsulates.^{34,35}

Accordingly, to improve the anti-melanoma effect of LUT, we constructed nano-delivery systems loaded with LUT using PPS-PEG as the nanocarrier. The anti-tumor activity of LUT-PPS-NPs was evaluated *in vitro* and *in vivo*. LUT-PPS-NPs with enhanced characteristics were synthesized utilizing an optimized titration and single emulsion solvent volatilization process, which increased LUT's aqueous solubility. The results demonstrated the effective production of ROS-responsive NPs loaded with LUT, from which LUT could be quickly released in a high ROS level environment. *In vitro* cell assays showed that the LUT-PPS-NPs could be significantly internalized by SK-MEL-28 cells. Moreover, LUT-PPS-NPs showed stronger anti-tumor effects in terms of anti-cell proliferation (low or normal density plating), migration and invasion, as well as promotion of apoptosis. The results of animal experiments revealed that intratumoral administration of LUT-PPS-NPs exhibited enhanced anti-melanoma activity compared to free LUT.

Materials and Methods

Materials

Luteolin (purity $\geq 98\%$) was purchased from the Shanghai Macklin Biochemical Co., Ltd. (Shanghai, China). Poly(propylene sulfide)-poly(ethylene glycol) (PPS-PEG) polymers and poly(propylene sulfide)-poly(ethylene glycol)-FITC (PPS-PEG-FITC) were purchased from Xi'an Ruixi Biological Technology Co., Ltd. (Xi'an, China). Penicillin, streptomycin, trypsin-EDTA and fetal bovine serum (FBS) were obtained from Gibco (Waltham, MA, USA). Phosphate-buffered saline (PBS), Dulbecco's Modified Eagle's Medium (DMEM), and Roswell Park Memorial Institute (RPMI)-

1640 for cell culture were purchased from HyClone Inc. (Waltham, MA, USA). The cell counting kit-8 (CCK-8) and apoptosis kit were purchased from Beyotime Biotechnology Co., Ltd. (Shanghai, China). Matrigel basement membrane matrix was purchased from Corning (New York, USA). All antibodies were from Cell Signaling Technology (Danvers, MA, USA).

Cell Lines and Cell Culture

The human malignant melanoma cell line (SK-MEL-28) was obtained from the American Type Culture Collection (ATCC, Rockville, MD, USA). Human skin fibroblasts (HSF) were obtained from the Kunming Institute of Zoology, CAS (Kunming, China). Throughout the study, SK-MEL-28 cells were cultured in RPMI-1640 supplemented with 10% FBS and 1% penicillin/streptomycin, while HSF were cultured in DMEM medium supplemented with 10% FBS and 1% penicillin/streptomycin, both in 5% CO₂ incubator at 37 °C.

Animals

Twenty-four female BALB/c nude mice (weighing approximately 20 g; age, 4-6 weeks) were purchased from Huachuang Sino Medical Technology Co., Ltd. (Jiangsu, China) and maintained under standard conditions. Animal experiments were approved by the Ethics Committee of Shanghai Skin Diseases Hospital. All animals were treated following the guidelines of the National Standard of the People's Republic of China (GB/T35892-2018) "Laboratory Animals - Guidelines for Ethical Review of Animal Welfare".

Preparation and Characterization of LUT-PPS-NPs

The LUT-loaded NPs (LUT-PPS-NPs) were prepared successively by two methods. The first preparation method used the double emulsion solvent volatilization method, in which 1 mg of LUT was dissolved in PBS (10 mL) at high temperature as aqueous phase 1, and then titrated into an oil phase consisting of 30 mg of PPS-PEG and 1 mL of dichloromethane. The aqueous phase 1 was mixed with the oil phase and then treated with intermittent sonication at 260 W for 1 min. Then the sonicated mixture was poured into 3 mL of 3% sodium cholate solution as aqueous phase 2, and after sonication again using the above procedure, the resulting oil-water emulsion was further diluted in 10 mL of 0.5% sodium cholate solution, and dichloromethane was removed by evaporation, during which NPs were generated by self-assembly. Finally, the LUT-PPS-NPs were centrifuged at 11,000 g for 30 min at 4°C, resuspended in sterile water and filtered through a 0.45 µm membrane and stored at 4°C away from light for subsequent use.

The second preparation was performed by the titration and single emulsion solvent volatilization method. 5 mg LUT and 30 mg PPS-PEG were dissolved in 2.5 mL acetone as the oil phase and 5 mL 3% sodium cholate solution as the aqueous phase, and the former was titrated into the latter, followed by the same sonication treatment as the first method for the mixture. The emulsion after sonication was further diluted with 10 mL 0.5% sodium cholate solution, and the organic matter was removed by rotary evaporation, followed by centrifugation at 11,000 g for 30 min at 4°C, and the product was resuspended and filtered through a 0.45 µm filter membrane, and the LUT-PPS-NPs were stored under the same conditions as described above for further study.

Thereafter, titration and single emulsion solvent volatilization method was used to prepare drug-free nanoparticles (PPS-NPs) and FITC fluorescein-labeled LUT-PPS-NPs (LUT-PPS-NPs-FITC). Notably, PPS-NPs were prepared without the addition of LUT, while LUT-PPS-NPs-FITC were produced with the application of PPS-PEG-FITC materials.

The particle size, zeta potential and polydispersity index (PDI) of LUT-PPS-NPs were measured by a Zetasizer Nano ZS (Malvern Instruments, United Kingdom) with three replicates in each test, while the morphology of LUT-PPS-NPs was determined by transmission electron microscopy (TEM, Hitachi, Tokyo, Japan).

Encapsulation Efficiency and Drug Loading

The amount of encapsulation was determined by the extraction method, 100 µL of NPs were dissolved in 2 mL of anhydrous ethanol, the NPs were decomposed by ultrasonication, centrifuged at 17,000 g for 10 min, and the absorbance of the supernatant was measured using an enzyme marker and the concentration of encapsulated LUT in NPs was calculated against the standard curve of free (unencapsulated) LUT in anhydrous ethanol, expressed as µg/mL.

Drug loading was determined as follows: first, a clean EP tube was obtained, baked at 80°C overnight and weighed, then 100 µL of NPs were added to the EP tube, baked at 80°C for 24 h and weighed, and the difference between the two masses was the dry weight of the NPs.

Encapsulation efficiency (EE) and Drug loading (DL) of LUT-PPS-NPs were calculated according to the following equations:

$$EE\% = \frac{\text{LUT amount encapsulated}}{\text{LUT amount initially added}} \times 100\%$$

$$DL\% = \frac{\text{LUT amount encapsulated}}{\text{Total weight of nanoparticles}} \times 100\%$$

In vitro Drug Release

100 µL of LUT-PPS-NPs were incubated in 500 µL of 10% FBS, PBS, and double-distilled water (with or without 500 µM H₂O₂) at 37°C. 200 µL of supernatant were centrifuged at a predetermined time point and supplemented with an equal amount of fresh solution. The absorbance of the supernatant at 350 nm was measured using an enzyme marker, and the amount of LUT released was calculated based on a pre-prepared standard curve. The release behavior of LUT from LUT-PPS-NPs was finally observed by plotting the cumulative release curve of LUT.

Cell Experiments

In vitro Cellular Uptake

Cellular uptake and intracellular drug distribution of LUT-PPS-NPs-FITC in SK-MEL-28 melanoma cells were detected by flow cytometry (FCM, BD Biosciences, Fortessa, CA, USA) and confocal laser scanning microscopy (CLSM, LSM-510, Carl Zeiss, Germany). The cells were seeded in 24-well plates at a density of 1×10^5 in complete medium. After overnight incubation, the medium was replaced with LUT-PPS-NPs-FITC and treated at different time points (1, 3, 6, 24 h), washed three times with PBS to remove residual LUT-PPS-NPs-FITC, followed by fixing the cells with 4% paraformaldehyde (PFA) for 20 min, washing three times and then treated with DAPI-containing anti-quencher. The results of cell internalization of NPs were then obtained using a confocal microscope and a flow cytometer.

Cellular Uptake Mechanism Assay

To investigate the internalization mechanism, the uptake experiments were performed with different inhibitors. SK-MEL-28 cells were seeded at a density of 5×10^5 in 6-well plates and incubated with chlorpromazine (CPZ, 15 µg/mL, clathrin-mediated endocytosis inhibitor), ethylisopropylamiloride (EIPA, 100 µM, inhibitor of macropinocytosis), nystatin (50 µg/mL, inhibitor of caveolae-mediated endocytosis) and nocodazole (2 µg/mL, microtubule inhibitors) for 45 min. Then, SK-MEL-28 cells were incubated with LUT-PPS-NPs-FITC for 3 h. After washing 3 times with PBS, the cells were collected and the FITC fluorescence intensity was analyzed by flow cytometer.

Cytotoxicity Assays

HSF and SK-MEL-28 cells were seeded in 96-well plates at a density of 1×10^4 and 8×10^3 cells/well, respectively. After cells were incubated overnight, they were treated with different concentrations of PPS-NPs, LUT and LUT-PPS-NPs solutions for 48 h. Control cells were treated with basal medium supplemented with 0.1% DMSO. Then the medium was removed from each well, and 100 µL of fresh medium containing 10 µL CCK-8 reagent was added. Cell viability was measured with the CCK-8 assay according to the manufacturer's instructions. Data were processed using GraphPad Prism software.

Cell Proliferation Inhibition Assays

SK-MEL-28 cells were also uniformly dispersed in 96-well plates at low density (8×10^2 cells/well) and normal density (8×10^3 cells/well) and treated with PPS-NPs, LUT and LUT-PPS-NPs for 10 days after adherence. The control group was

treated with basal medium RPMI-1640 containing 0.1% DMSO. Cell proliferation was detected after 10 days of co-incubation using the CCK-8 assay.

Apoptosis Assays

The SK-MEL-28 cells were seeded in 6-well plates (3×10^5 cells/well), and on the following day, they were treated with the indicated concentrations of drugs for 48 h. Supernatant and adherent cells were collected, rinsed with PBS and resuspended in binding buffer. Annexin V-FITC and PI were added and incubated at room temperature for 15-20 min. The samples were then analyzed within 1 h by flow cytometer.

Cell Migration-Wound-Healing Assays

In vitro wound-healing assay was used to observe the migration of SK-MEL-28 cells after LUT/LUT-PPS-NPs treatment. The cells were seeded at 9×10^5 cells/well into 6-well plates. The center of the cell monolayer was then scraped using a sterile yellow pipette tip (Axygen, USA) to create a straight gap of constant width. The wells were washed with PBS and then exposed to PPS-NPs, LUT and LUT-PPS-NPs at appointed concentrations for 48 h. Wound closure was imaged at 0 and 48 h using an inverted light microscope (magnification $\times 50$) (Carl Zeiss, Germany). Photographs of 5 independent areas were taken, and the areas of migration were quantified using ImageJ software. The results are reported as percent of migration rate, calculated using the formula:

$$\text{Migration rate(\%)} = \frac{\text{Area of 0h} - \text{Area of 48 h}}{\text{Area of 0h}} \times 100\%$$

Cell Invasion-Transwell Assays

Cell invasion ability was tested using a commercial Transwell system (24-well plates, 8.0 μm pore size, Costar, IL, USA). Transwell upper inserts were coated with 0.1 mL of diluted Matrigel and incubated for 3 h at 37°C, then 0.2 mL of the PPS-NPs, LUT and LUT-PPS-NPs in warm (37°C) serum-free medium was added to melanoma cells (2×10^5) seeded in the upper wells of 24-well Transwell plates. The lower wells contained complete medium with 20% FBS. After 48 h incubation in a humidified 5% CO_2 atmosphere, the upper well content (non-invading cells) was removed, the inserts were washed with PBS and cells were fixed with 4% paraformaldehyde at 37°C for 30 min. The cells were washed three times with PBS and stained with 0.05% crystal violet for 15 min. Fields were selected at random, observed using an inverted light microscope and quantified by manual counting.

Animal Experiments

In vivo Anticancer Therapy

A cell suspension of 100 μL PBS containing 2×10^6 SK-MEL-28 cells was injected subcutaneously into the right abdomen of female BALB/c nude mice. When the tumor reached approximately 70 mm^3 , 21 days after subcutaneous injection of tumor cells, drug administration was started and recorded as “day 0”.

The tumor-bearing mice were divided into 4 groups ($n = 6$ per group): (I) PBS, (II) PPS-NPs, (III) LUT (4 mg/kg), and (IV) LUT-PPS-NPs (4 mg/kg). Intratumoral administration was performed after measuring tumor size and weight every other day until the end of the trial. Tumor volume (V) was calculated as $V (\text{mm}^3) = 1/2 \times \text{length} \times \text{width}^2$. The mice were euthanized after 14 days. The tumors were then isolated, weighed, and photographed. The isolated tumors and main organs (heart, liver, spleen, lung, and kidney) were fixed in 4% paraformaldehyde, paraffin-embedded, and slices were stained with hematoxylin-eosin (H&E), TUNEL, Ki-67, and CD31.

Statistical Analysis

Values are presented as the mean \pm standard deviation (SD). Student's t -tests and two-way ANOVA with Bonferroni correction were used for statistical analysis. All statistical analyses were performed using GraphPad Prism software. Statistical significance was set at $P < 0.05$.

Table 1 Physicochemical Properties of LUT-PPS-NPs Prepared by Different Methods

Preparation Method	EE (%)	DL (w/w, %)	Size (nm)	PDI	Zeta Potential (mV)
First method ^a	16.19 ± 8.98	1.68 ± 1.00	196 ± 1.35	0.07 ± 0.05	−24.7 ± 1.93
Second method ^b	40.15 ± 0.19	15.05 ± 0.07	169.77 ± 7.33	0.28 ± 0.04	−15.63 ± 0.98

Notes: ^aFirst method refers to the double emulsion solvent volatilization method. ^bSecond method refers to the titration and single emulsion solvent volatilization method.

Abbreviations: PDI, polydispersity index; EE, encapsulation efficiency; DL, drug loading.

Results

Preparation and Characterization of LUT-PPS-NPs

The LUT-PPS-NPs were prepared by the double emulsion solvent volatilization, and the titration and single emulsion solvent volatilization methods, and the NP products were characterized in terms of drug loading (DL)%, encapsulation rate (EE)% particle size, PDI and zeta potential (Table 1). A schematic diagram of the synthesis of LUT-PPS-NPs prepared by the titration and single emulsion volatilization method is shown in Figure 1A. Higher encapsulation ($40.15 \pm 0.19\%$) and loading rates ($15.05 \pm 0.07\%$) were obtained using the titration and single emulsion solvent volatilization method for the preparation of LUT-PPS-NPs, which is consistent with the easier dissolution of LUT in acetone than in PBS. The PDI value (0.28 ± 0.04) indicated good dispersion of LUT-PPS-NPs along with small particle size (169.77 ± 7.33 nm), and the zeta potential showed that the NPs were negatively charged (Figure 1B and C). The particle size of PPS-NPs was 157.2 ± 6.19 nm by DLS (results not shown), indicating that the loading of LUT did not have much effect on the particle size of NPs. TEM was used to characterize the physicochemical properties of the LUT-PPS-NPs (Figure 1D), and the images show that the nanoparticles are spherical with a typical core-shell structure with a size of about 143.66 ± 4.79 nm. This size is slightly smaller than the DLS test results, which is because the LUT-PPS-NPs are in the dry collapsed state during the TEM test, while in the DLS test, the LUT-PPS-NPs are in the dispersed hydrated state. In summary, we chose the titration and single emulsion solvent volatilization method rather than the double emulsion solvent volatilization method for subsequent study.

In vitro Drug Release of LUT-PPS-NPs

Compared to PBS, LUT-PPS-NPs released only about 30% of LUT within 75 h in 10% FBS (Figure 1E) and entered a plateau thereafter, indicating that LUT-PPS-NPs released only a small amount of LUT in the normal cellular environment.

On the contrary, after the addition of 500 μM H_2O_2 (simulating a high-ROS environment in the tumor), cumulative release of LUT was approximately 98% within 72 h (Figure 1F), indicating a triggering effect of H_2O_2 on drug release. The morphological changes in PPS-NPs under a high ROS environment were analyzed using TEM, as shown in Figure 1G. At the same concentration of H_2O_2 , the aggregation and disintegration of NPs appeared at 24 h, most of the NPs disintegrated at 48 h, and almost completely disintegrated at 48 h under high H_2O_2 level. Our results indicate that LUT-PPS-NPs are ROS-responsive, have good stability under physiological settings, and may conduct regulated release of LUT at lesion locations with high H_2O_2 levels.

In vitro Cellular Uptake and Mechanisms

To investigate the cellular uptake efficiency of LUT-PPS-NPs, the cellular uptake of LUT-PPS-NPs-FITC by SK-MEL-28 melanoma cells was observed. Under confocal laser scanning microscopy, the cytoplasm showed green fluorescence after co-incubation with LUT-PPS-NPs-FITC, confirming the accumulation of NPs in the cells over time (Figure 2A). Quantitative flow cytometric analysis demonstrated that LUT-PPS-NPs-FITC were rapidly taken up by SK-MEL-28 cells from 1 h and the uptake of fluorescent NPs was positively correlated with time (Figure 2B and C), with the highest uptake of LUT-PPS-NPs-FITC at 24 h compared to 1 h, 3 h or 6 h after incubation.

In addition, the uptake mechanism of LUT-PPS-NPs by SK-MEL-28 melanoma cells was investigated by several endocytosis inhibitors including CPZ (clathrin-mediated endocytosis inhibitor), EIPA (inhibitor of macropinocytosis), nystatin (inhibitor of caveolae-mediated endocytosis) and nocodazole (microtubule inhibitors) using the inhibitor methods. The result showed no obvious change in the fluorescence intensity of cells treated with CPZ, EIPA and nystatin, while the fluorescence intensity of cells treated with nocodazole was significantly reduced. Microtubules are involved in vesicular trafficking and nocodazole as a microtubule inhibitor can inhibit the endocytotic trafficking

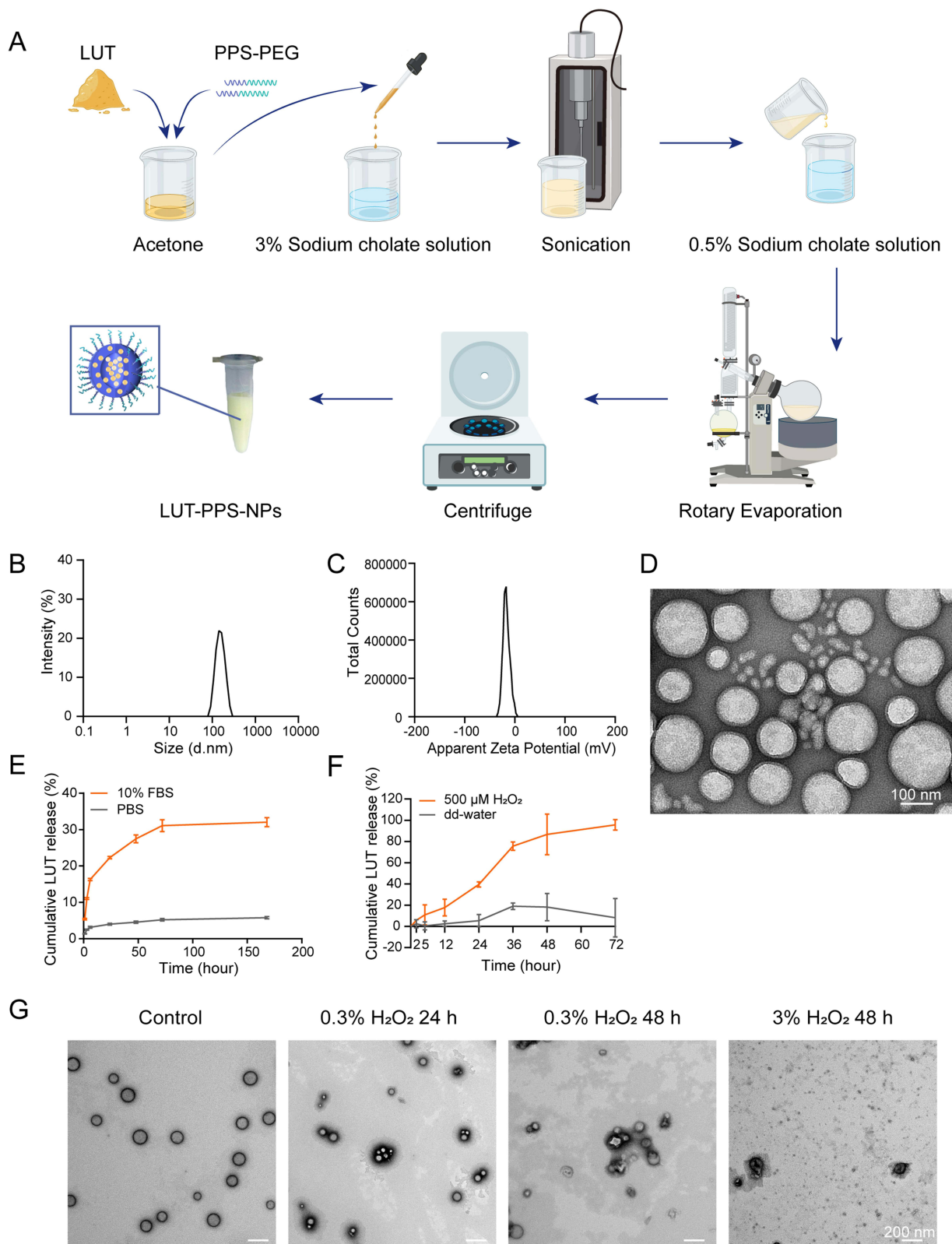


Figure 1 Preparation and characterization of LUT-PPS-NPs. **(A)** Schematic diagram showing the process of preparing LUT-PPS-NPs by titration and single emulsion solvent volatilization method. **(B and C)** Size distribution and zeta potential of LUT-PPS-NPs. **(D)** Morphology of LUT-PPS-NPs observed by TEM. **(E and F)** In vitro drug release behavior of LUT from LUT-PPS-NPs in 10% FBS, PBS or 500 μ M H_2O_2 ($n = 3$). **(G)** Electron micrographs of PPS-NPs degradation after hydrogen peroxide treatment.

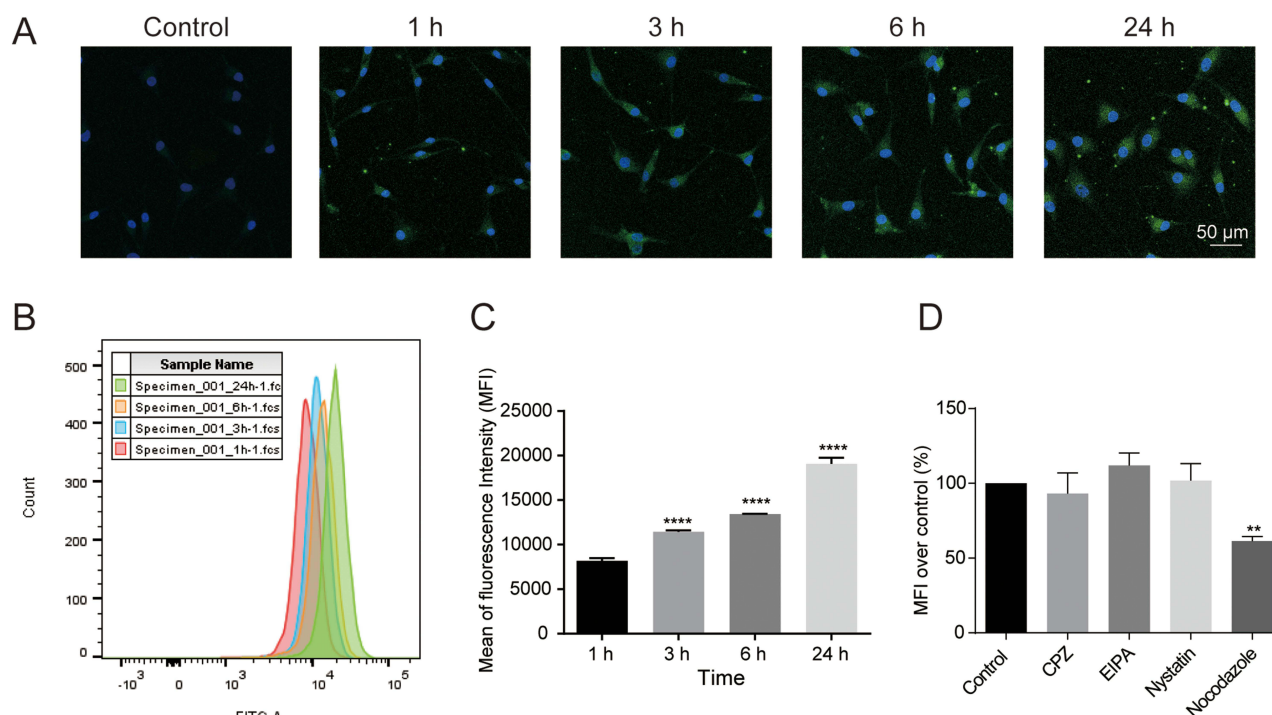


Figure 2 Cellular uptake of FITC-labeled LUT-PPS-NPs in SK-MEL-28 cells. **(A)** Confocal images of cell internalization at different times. **(B)** Flow cytometric analysis. **(C)** Mean fluorescence intensity of SK-MEL-28 cellular uptake detected by flow cytometry ($n = 3$). Compared to 1 h, **** $p < 0.0001$. **(D)** Analysis of cellular uptake mechanisms ($n = 3$). Compared to control, ** $p < 0.01$.

pathway, so the result suggests that the uptake of LUT-PPS-NPs by SK-MEL-28 cells is closely related to microtubules (Figure 2D).

In vitro Cytotoxicity Assays

To investigate the anti-tumor activity of LUT-PPS-NPs, the cytotoxicity of different drug treatments on HSF and SK-MEL-28 cells was examined firstly by the CCK-8 assay. At the same LUT concentration, the survival rate of HSF was more than 75% after LUT-PPS-NPs treatment (Figure 3A). This implies that the cytotoxicity of LUT-PPS-NPs on normal skin cells was negligible under low concentration administration compared to free LUT. Figure 3B shows that PPS-NPs had no in vitro anticancer activity. However, the viability of SK-MEL-28 cells treated with LUT and LUT-PPS-NPs decreased with increased drug concentration. The IC₅₀ values for LUT and LUT-PPS-NPs were 12.37 μ M and 13.92 μ M, respectively. Furthermore, LUT-PPS-NPs exerted more potent tumor cell killing effects following administration of the same low concentration. These results suggest that LUT-PPS-NPs can effectively and selectively kill melanoma cells without harming normal skin cells.

Cell Apoptosis Assays

To further investigate the anti-tumor effects of LUT-PPS-NPs, the apoptosis of SK-MEL-28 cells was examined by flow cytometry, with dead cells labeled with PI and apoptotic cells labeled with Annexin V (Figure 3D). With increased drug concentration, the apoptosis rate caused by LUT-PPS-NPs also gradually increased. The results showed that the drug-loaded NPs caused a higher apoptosis rate and exerted a stronger tumor-killing effect compared to the same concentration of the LUT group, which is consistent with the cytotoxicity assays. At the concentration of 10 μ M, the total apoptosis rate caused by LUT-PPS-NPs was 2 times that of LUT (Figure 3C).

Cell Proliferation Inhibition Effect

Bioinformatics analysis in the study of John Schomberg et al¹⁵ showed that LUT downregulated the ECM gene in melanoma (including SK-MEL-28 cells) and that LUT-mediated ECM had an impact on density-dependent cell survival.

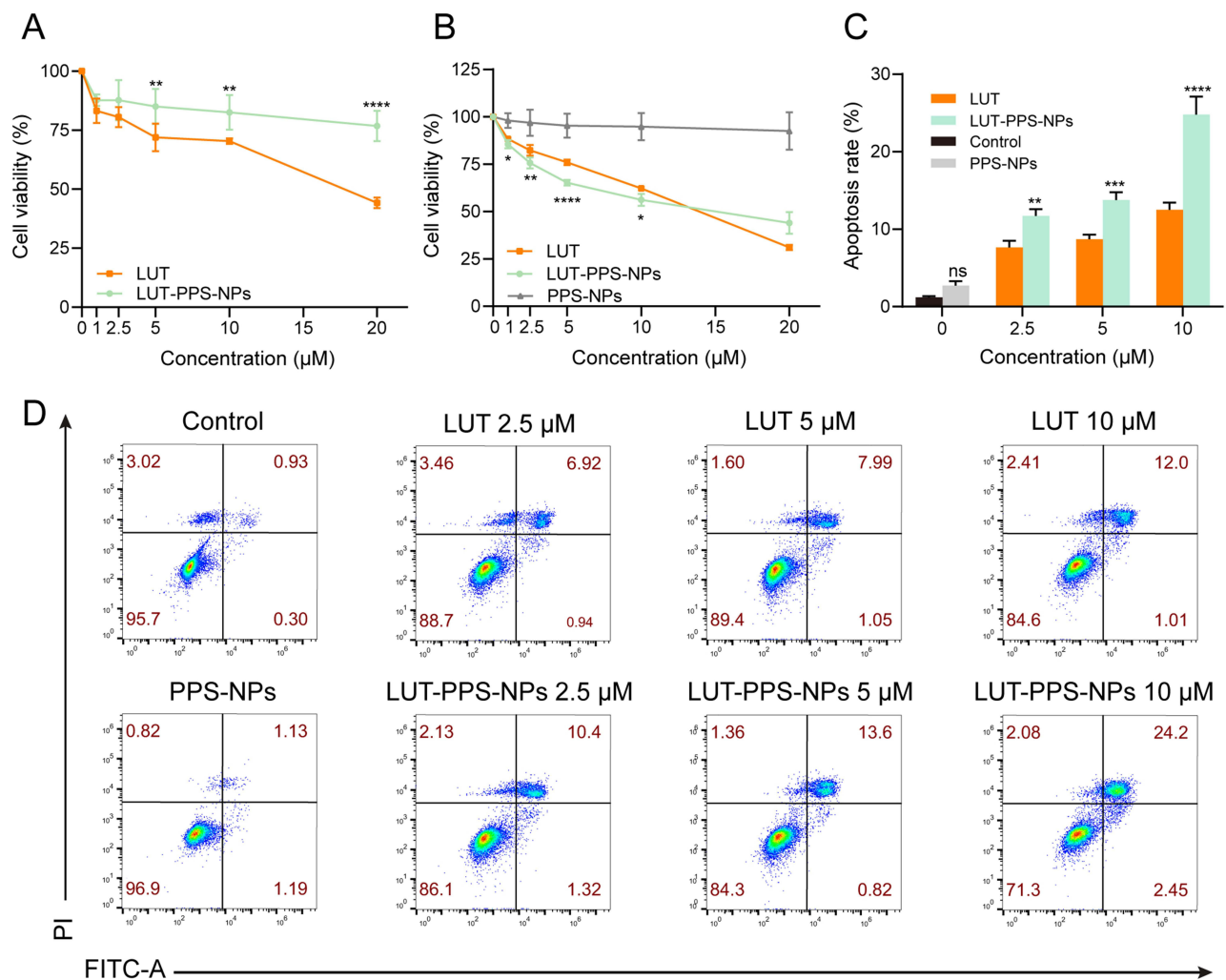


Figure 3 Cytotoxicity and flow cytometry apoptosis analysis of LUT-PPS-NPs (A) Cytotoxicity of LUT/LUT-PPS-NPs on HSF (n = 5). (B) Viability of SK-MEL-28 cells treated with PPS-NPs, LUT and LUT-PPS-NPs for 48 h (n = 5). (C) Flow cytometry detection of apoptosis rate after different treatments (n = 3). NS means no significance, compared with control. *p < 0.05, **p < 0.01, ***p < 0.001, ****p < 0.0001 compared with the LUT at the same concentration. (D) Flow Cytometry Apoptosis Images.

Considering that low fibronectin accumulation is associated with low-density cells, it is closely related to ECM-mediated proliferation and/or cell death. They used SK-MEL-28 and WM3211 melanoma cells for cell density-related proliferation inhibition assays, which was shown that LUT inhibited the proliferation of low-density melanoma cells more strongly than normal-density cells. Inspired by this, we used a lower plate density (8×10^2 cells/well) relative to the normal plate density of CCK-8 assay (8×10^3 cells/well) for proliferation inhibition experiments based on pre-experiments.

Figure 4 shows that at the same dose, the proliferation inhibitory effect of LUT-PPS-NPs on tumor cells was stronger than LUT at all concentrations for low density SK-MEL-28 cells (Figure 4A and C). After 10 days of co-incubation, whether the cells were low-density or normal-density, the suppression of tumor proliferation by LUT-PPS-NPs was greater as the drug concentration increased. SK-MEL-28 cell growth was completely inhibited under LUT-PPS-NPs treatment compared with the LUT 20 μM group (including low-density Figure 4A and C and normal-density Figure 4B and D). It has been shown that intracellular ROS levels were significantly higher in circulating melanoma cells and visceral metastatic nodules compared to subcutaneous tumors,³⁶ and the above results suggest that LUT-PPS-NPs may be able to exert a stronger anti-melanoma metastatic effect. In conclusion, LUT-PPS-NPs had a higher anti-tumor cell proliferation impact in vitro than free LUT in the event of long-term treatment, which was more obvious in the case of low-density cancer cells.

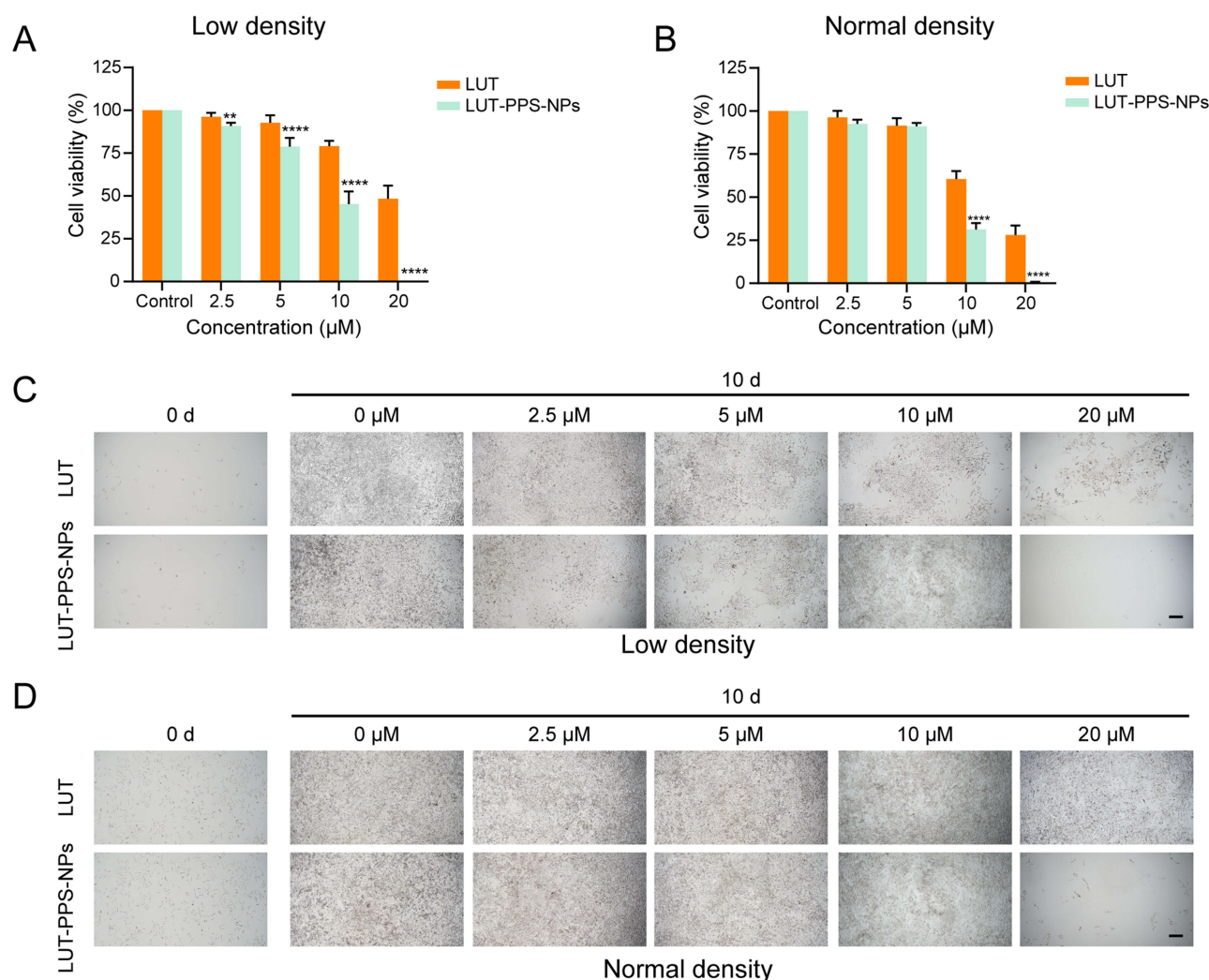


Figure 4 Proliferation inhibition of LUT/LUT-PPS-NPs on low density cells and normal density cells. **(A and C)** Proliferation of low density seeded SK-MEL-28 cells after 10 days of LUT/LUT-PPS-NPs treatment. **(A)** Quantitative results of C by CCK-8 assay ($n = 5$). **(B and D)** Proliferation of normal density seeded SK-MEL-28 cells after 10 days of LUT/LUT-PPS-NPs treatment. **(B)** Quantitative results of D by CCK-8 assay ($n = 5$). Images were taken under an inverted microscope at 50x magnification. The scale bar is 200 μm . ** $P < 0.01$, **** $P < 0.0001$ compared with the LUT at the same concentration.

Cell Migration and Invasion Assays

The migration and invasion of tumor cells are tightly related to tumor metastasis. Firstly, the wound-healing assay was performed to simulate the effect of the drug on the horizontal migration ability of tumor cells (Figure 5A and B). A low concentration of LUT-PPS-NPs exerted stronger tumor migration resistance than the same concentration of LUT, and the cell migration activity was significantly inhibited with increasing concentration. The migration rate of SK-MEL-28 cells treated with 10 μM LUT-PPS-NPs for 48 h was only about 10%. Cell invasion assay results were consistent with the migration assay results (Figure 5C and D). The number of cells crossing the stromal gel gradually decreased with increasing drug concentration, while the transmigration cell number in the LUT-PPS-NPs group was significantly lower than that in the free LUT group at the same concentration. The above results showed that LUT-PPS-NPs inhibited the motility of melanoma cells more effectively.

In vivo Anticancer Therapy

Considering LUT-PPS-NPs had such good anti-tumor activity in vitro, we adopted the nude mouse xenograft model to investigate the tumor suppression effect of NPs in vivo. Figure 6A depicts the in vivo animal experimental method in brief. The tumor-bearing mice were randomly separated into four groups and treated with intratumoral injection every

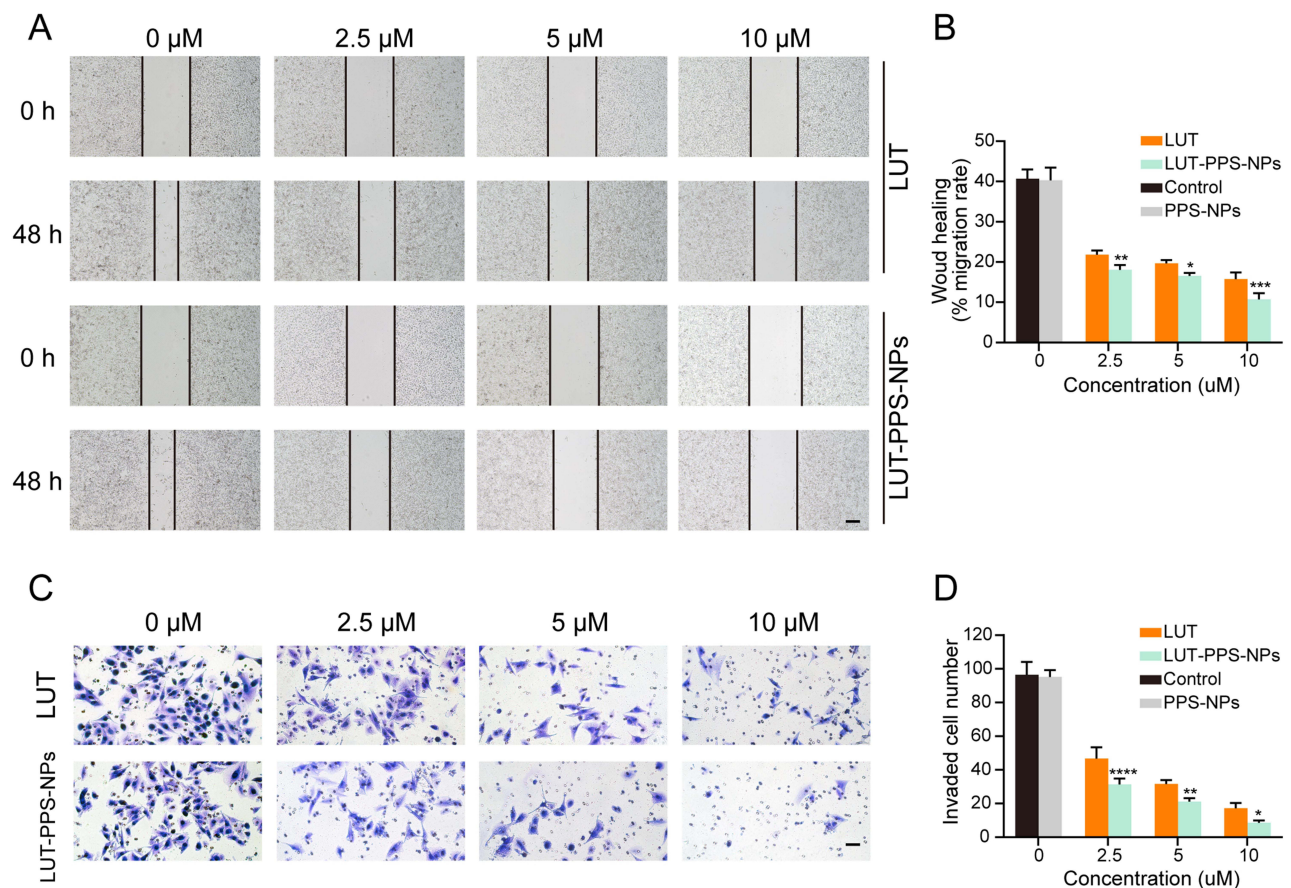


Figure 5 Migration and invasion of SK-MEL-28 cells. **(A and B)** Wound-healing of SK-MEL-28 cells treated with the same concentration of LUT or LUT-PPS-NPs for 48 hours ($n = 5$). Images were taken under an inverted microscope at 50x magnification and the area of the scratches was measured. The scale bar is 200 μm . **(C and D)** SK-MEL-28 cells were treated with the same concentration of LUT or LUT-PPS-NPs for 48 h to observe cell invasion ($n = 5$). Images were taken at 200x magnification under an inverted microscope and the number of transmembrane cells in five random regions was determined. The scale bar was 50 μm . * $P < 0.05$, ** $P < 0.01$, *** $P < 0.001$, **** $P < 0.0001$ compared with the LUT at the same concentration.

two days after the SK-MEL-28 nude mouse melanoma model was established. Throughout the trial, body weight and tumor growth were monitored and documented. The mice were sacrificed and the tumor tissues were extracted for further research after 7 administrations (**Figure 6B and C**). As shown in **Figure 6D**, tumor volume rose consistently in both the PBS and PPS-NPs treatment groups, and there was no statistically significant difference in tumor size between the two groups of mice, showing that blank PPS-NPs had no anticancer action. Compared with the control group (PBS group), the LUT group was apparently able to inhibit melanoma growth, indicating that LUT has a strong anti-melanoma effect *in vivo*. Following treatment, the tumor size in the group receiving LUT-PPS-NPs was substantially smaller than that in the group receiving LUT, with the difference being statistically significant. Also, the tumor weight of the isolated LUT-PPS-NPs group at the end of the experiment was approximately half of that of the free LUT group (**Figure 6E**). These results suggest that LUT-PPS-NPs exhibit stronger *in vivo* antitumor effects. On the other hand, the weight changes across the treatment groups were not significant (**Figure 6F**).

The improved anti-tumor effect of LUT-PPS-NPs was further verified by H&E, TUNEL, Ki67 and CD31 staining assays (**Figure 6G**). Among all groups, the LUT-PPS-NPs group showed the most significant anti-tumor effect, with more extensive necrosis in the tumor area in the H&E stained image, the most extensive apoptosis in the TUNEL fluorescence image, the least number of positive cells in the Ki67 stained image and less CD31 positive staining. These results suggest that LUT-PPS-NPs may effectively inhibit tumor growth *in vivo* by inducing apoptosis, inhibiting cell proliferation and angiogenesis.

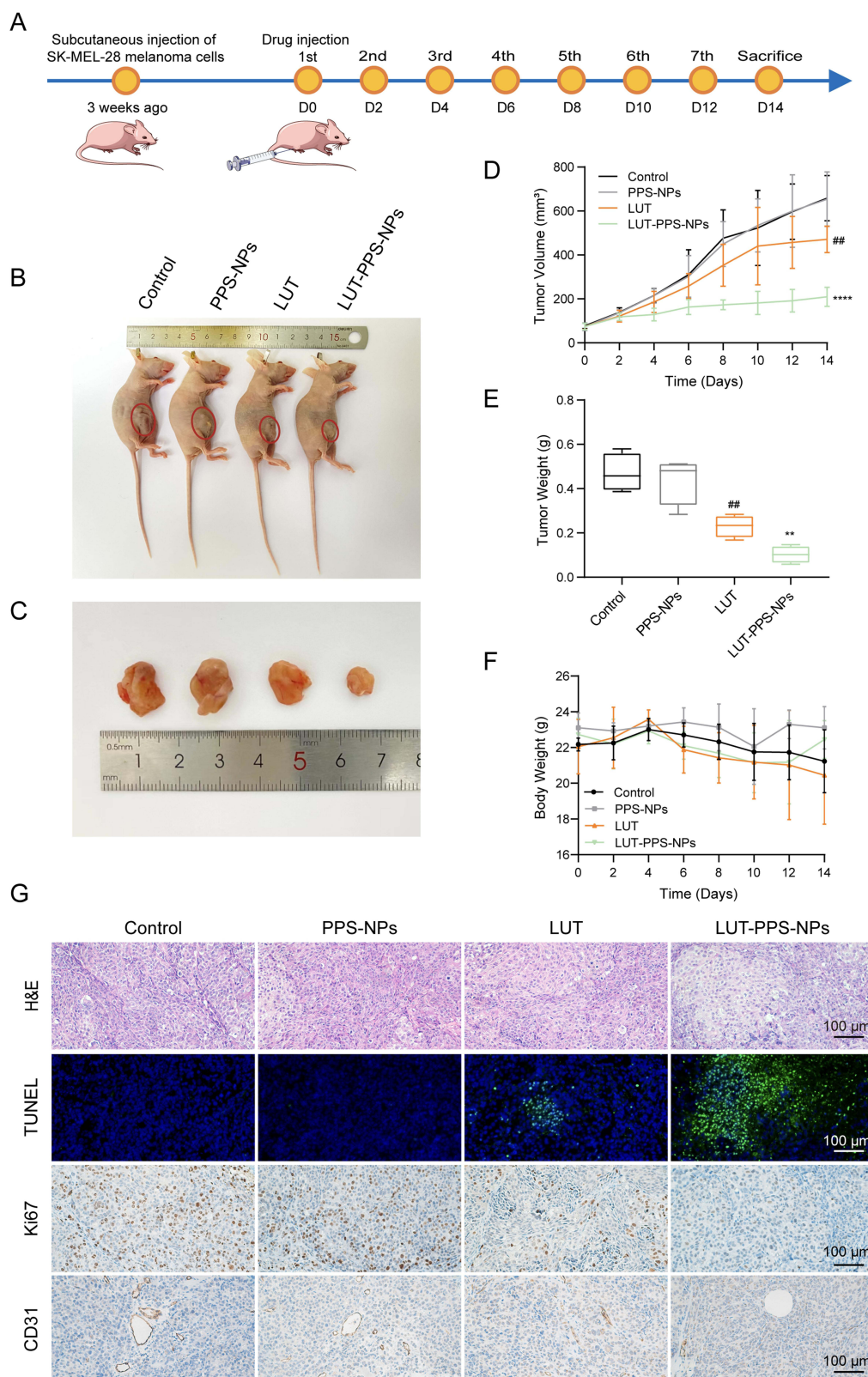


Figure 6 In vivo antitumor efficacy and histological analysis. **(A)** Schematic diagram of in vivo experimental procedure. **(B)** Photographs of tumor-bearing mice at the end of the experiment. Mice received 4 mg/kg of LUT or 4 mg/kg of LUT in LUT-PPS-NPs every two days. **(C)** Photo of the collected SK-MEL-28 tumors at Day 14. **(D)** Tumor growth curves of SK-MEL-28 tumor-bearing nude mice injected intratumorally with PBS, PPS-NPs, LUT and LUT-PPS-NPs for 14 days (n=4). **(E)** Weight of SK-MEL-28 tumors at Day 14 (n = 4). **(F)** Body weight curves of BALB/c mice measured every two days (n = 4). Day 0 indicates treatment initiation. Error bars represent SD of at least three replicates. **(G)** Pathological section analysis of tumor tissues. **P < 0.01, ****P < 0.0001 compared with the LUT. ###P < 0.01 compared with control.

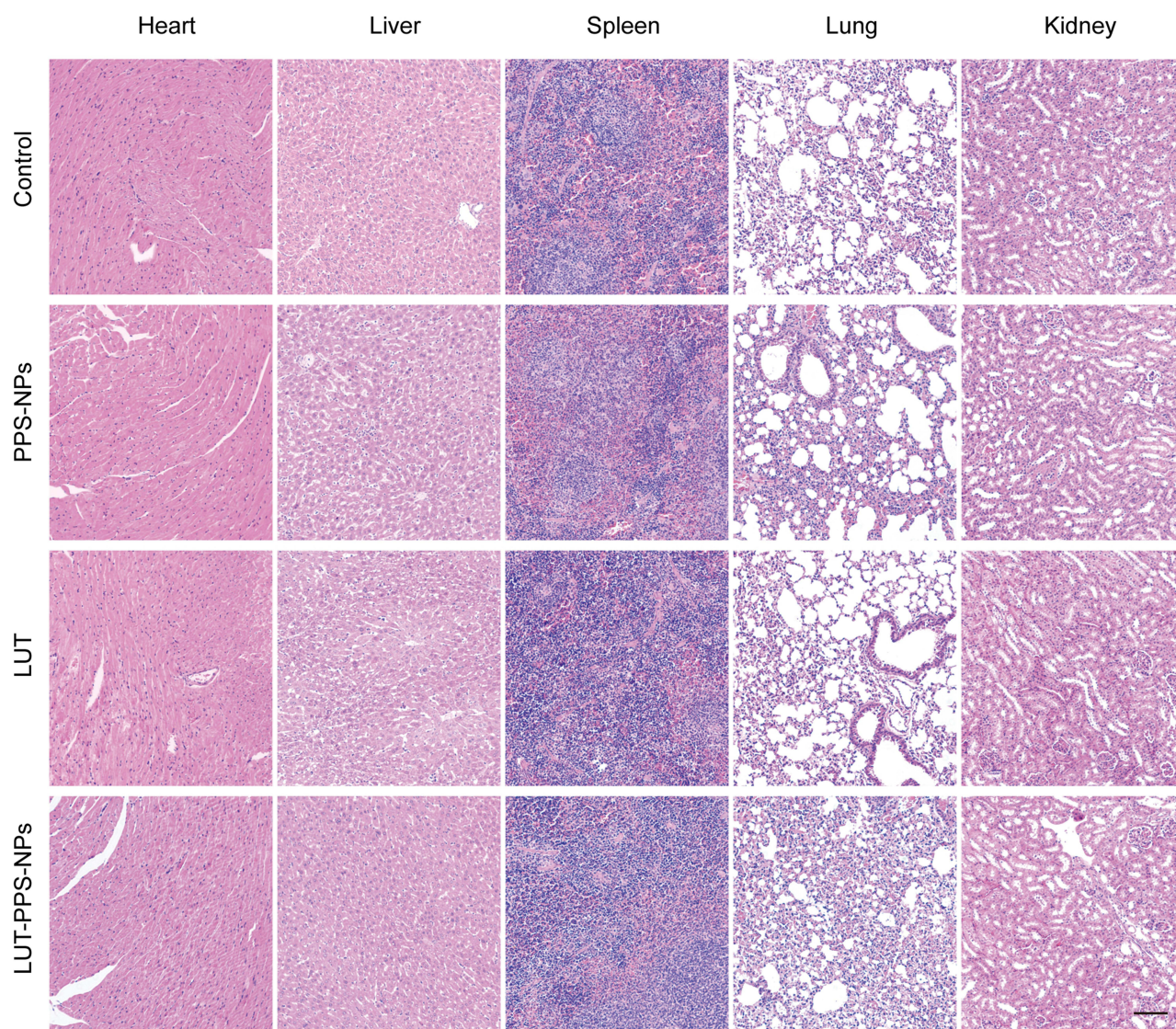


Figure 7 In vivo experimental visceral toxicity analysis. H&E staining sections of major organs (heart, liver, spleen, lung and kidney) in each group. Images were taken at 200× magnification under an inverted microscope. The scale bar is 100 μ m.

The biological safety of LUT-PPS-NPs in vivo was preliminarily investigated by histological analysis. There was no obvious morphological/histological damage in the main organs (Figure 7), which may be due to the use of intratumoral administration to reduce systemic diffusion of the drugs.

Discussion

Nanotechnology allows the preparation of hydrophobic LUT into water-soluble nano-LUT and its entry into cells by direct diffusion through the cytoplasmic membrane and receptor-mediated endocytosis.^{37,38} In terms of the nano-delivery of LUT, materials used in current studies to improve the bioavailability and efficacy include nanoparticles,^{39,40} micelles,⁴¹ liposomes,⁴² and nanoemulsions.⁴³ However, limitations of the current investigation include the fact that the biological efficacy of LUT-loaded nano preparations has not been systematically evaluated and that there is a lack of LUT nano-drug delivery methods in melanoma treatment studies.

Given the close relationship between ROS and melanoma, as well as the presence of high levels of ROS in melanoma cells,^{44–46} we prepared NPs using the ROS-responsive material PPS-PEG to increase the water solubility of LUT and promote its release in melanoma cells, thereby enhancing its anti-melanoma effect. Where PPS wrapped the hydrophobic

drug LUT inside the NPs to form a hydrophobic inner core, which could exhibit a phase transition from hydrophobic to the hydrophilic state under oxidizing conditions in melanoma tissues, the nanoparticles were easily degraded during the phase transition, leading to the release of LUT. Moreover, PEG was used to generate a hydrophilic surface on the outer surface of the nanoparticles, which increased their water solubility.^{47,48} Notably, a more efficient titration and single emulsion solution volatilization method was chosen to prepare LUT-PPS-NPs using the characteristics of LUT with high solubility in acetone.

In the cytotoxicity study, LUT-PPS-NPs showed a lower cytotoxic effect on HSF and higher cytotoxicity on SK-MEL-28 tumor cells compared to the same concentration of free LUT, which may be due to the higher ROS level in SK-MEL-28 cells compared to normal skin cells, making the NPs easier to enter SK-MEL-28 cells and successfully release LUT, thus reducing the toxicity to normal cells while exerting anti-tumor effects. Remarkably this ROS-stimulating decomposition property of LUT-PPS-NPs was confirmed in drug release experiments and TEM image observations.

In terms of the anti-tumor effect, apoptosis, proliferation, migration and invasion assays further demonstrated the in vitro anti-tumor advantage of LUT-PPS-NPs. It is important to highlight that under prolonged administration, LUT-PPS-NPs exerted more anti-tumor cell proliferation than free LUT, which was particularly evident in low-density cells. This result may be due to greater stability of the NPs, whose slow-release properties enhance more efficient tumor suppression under prolonged drug action and reduce the number of doses administered. It has been shown that LUT can inhibit the extracellular matrix pathway of tumor cells, while low-density cells can be analogized to a lower extracellular matrix where aggregated cells need to generate sufficient ECM density to support normal cell proliferation, and this property of LUT indicates its potential role in killing cancer cells in a low aggregated state.^{15,49–51} Moreover, combined with the results of migration and invasion assays, LUT-PPS-NPs undoubtedly have more potential advantages in anti-tumor metastasis.

Finally, the melanoma transplantation tumor model further illustrated the anti-tumor effect of LUT-PPS-NPs in vivo. Tumor growth was significantly inhibited in water-soluble nano-LUT-treated nude mice compared to the LUT group. The immunofluorescence and immunohistochemistry results of isolated tumor tissues further confirmed the more effective anti-tumor effects of LUT-PPS-NPs than free LUT. Pathological section analysis of key organs revealed no significant drug toxicity, likely as a result of the intratumoral administration reducing systemic response.^{52,53}

Conclusion

In summary, we developed LUT-loaded NPs using the ROS-responsive material PPS-PEG to overcome the low water solubility and low bioavailability of LUT and to improve the anti-melanoma effect in vitro and in vivo. The prepared LUT-PPS-NPs had a spherical structure, were ROS-responsive, and could be effectively internalized by SK-MEL-28 melanoma cells. Our study clearly demonstrated that LUT-PPS-NPs exerted more effective anti-melanoma effects in vitro and in vivo compared to free LUT. Although the exact mechanism needs to be further investigated, this delivery system provides a novel strategy to enhance the anti-melanoma activity of flavonoid phytopharmaceuticals such as LUT.

Acknowledgments

This study was supported by grants from the Program of the Science and Technology Commission of Shanghai Municipality “Science and Technology Innovation Action Plan” Medical Innovation Research Special Project (Grant/Award Number: 22Y11905700), Anhui Provincial Education Department Scientific Research Project (Grant/Award Number: YJS20210323) and Program of Shanghai Municipal Health Commission (Grant/Award Number: 2020YJZX0108).

Disclosure

The authors report no conflicts of interest in this work.

References

1. Schadendorf D, Fisher DE, Garbe C, et al. Melanoma. *Nat Rev Dis Primers*. 2015;1:15003. doi:10.1038/nrdp.2015.3
2. Luke JJ, Flaherty KT, Ribas A, Long GV. Targeted agents and immunotherapies: optimizing outcomes in melanoma. *Nat Rev Clin Oncol*. 2017;14(8):463–482. doi:10.1038/nrclinonc.2017.43

3. Kudchadkar RR, Lowe MC, Khan MK, McBrien SM. Metastatic melanoma. *CA Cancer J Clin.* 2020;70(2):78–85. doi:10.3322/caac.21599
4. Amaria RN, Menzies AM, Burton EM, et al. Neoadjuvant systemic therapy in melanoma: recommendations of the international neoadjuvant melanoma consortium. *Lancet Oncol.* 2019;20(7):e378–e389. doi:10.1016/S1470-2045(19)30332-8
5. Coit DG, Thompson JA, Algazi A, et al. Melanoma, version 2.2016, NCCN clinical practice guidelines in oncology. *J Natl Compr Canc Netw.* 2016;14(4):450–473. doi:10.6004/jnccn.2016.0051
6. Iqbal J, Abbasi BA, Ahmad R, et al. Potential phytochemicals in the fight against skin cancer: current landscape and future perspectives. *Biomed Pharmacother.* 2019;109:1381–1393. doi:10.1016/j.biopha.2018.10.107
7. Theoharides TC, Cholevas C, Polyzoidis K, Politis A. Long-COVID syndrome-associated brain fog and chemofog: luteolin to the rescue. *Biofactors.* 2021;47(2):232–241. doi:10.1002/biof.1726
8. Imran M, Rauf A, Abu-Izneid T, et al. Luteolin, a flavonoid, as an anticancer agent: a review. *Biomed Pharmacother.* 2019;112:108612. doi:10.1016/j.biopha.2019.108612
9. Gendrisch F, Esser PR, Schempp CM, Wölfl U. Luteolin as a modulator of skin aging and inflammation. *Biofactors.* 2021;47(2):170–180. doi:10.1002/biof.1699
10. Aziz N, Kim MY, Cho JY. Anti-inflammatory effects of luteolin: a review of in vitro, in vivo, and in silico studies. *J Ethnopharmacol.* 2018;225:342–358. doi:10.1016/j.jep.2018.05.019
11. Ganai SA, Sheikh FA, Baba ZA, Mir MA, Mantoo MA, Yattoo MA. Anticancer activity of the plant flavonoid luteolin against preclinical models of various cancers and insights on different signalling mechanisms modulated. *Phytother Res.* 2021;35(7):3509–3532. doi:10.1002/ptr.7044
12. Juszcak AM, Wöelfle U, Končić MZ, Tomczyk M. Skin cancer, including related pathways and therapy and the role of luteolin derivatives as potential therapeutics. *Med Res Rev.* 2022;42(4):1423–1462. doi:10.1002/med.21880
13. Juszcak AM, Czarnomysy R, Strawa JW, Zovko Končić M, Bielawski K, Tomczyk M. In vitro anticancer potential of jasione montana and its main components against human amelanotic melanoma cells. *Int J Mol Sci.* 2021;22(7):3345. doi:10.3390/ijms22073345
14. Yao X, Jiang W, Yu D, Yan Z. Luteolin inhibits proliferation and induces apoptosis of human melanoma cells in vivo and in vitro by suppressing MMP-2 and MMP-9 through the PI3K/AKT pathway. *Food Funct.* 2019;10(2):703–712. doi:10.1039/c8fo02013b
15. Schomberg J, Wang Z, Farhat A, et al. Luteolin inhibits melanoma growth in vitro and in vivo via regulating ECM and oncogenic pathways but not ROS. *Biochem Pharmacol.* 2020;177:114025. doi:10.1016/j.bcp.2020.114025
16. Tian L, Wang S, Jiang S, et al. Luteolin as an adjuvant effectively enhances CTL anti-tumor response in B16F10 mouse model. *Int Immunopharmacol.* 2021;94:107441. doi:10.1016/j.intimp.2021.107441
17. Huang M, Su E, Zheng F, Tan C. Encapsulation of flavonoids in liposomal delivery systems: the case of quercetin, kaempferol and luteolin. *Food Funct.* 2017;8(9):3198–3208. doi:10.1039/c7fo00508c
18. Lin LC, Pai YF, Tsai TH. Isolation of luteolin and luteolin-7-O-glucoside from dendranthema morifolium ramat tzvel and their pharmacokinetics in rats. *J Agric Food Chem.* 2015;63(35):7700–7706. doi:10.1021/jf505848z
19. Mitchell MJ, Billingsley MM, Haley RM, Wechsler ME, Peppas NA, Langer R. Engineering precision nanoparticles for drug delivery. *Nat Rev Drug Discov.* 2021;20(2):101–124. doi:10.1038/s41573-020-0090-8
20. Xin Y, Huang M, Guo WW, Huang Q, Zhang LZ, Jiang G. Nano-based delivery of RNAi in cancer therapy. *Mol Cancer.* 2017;16(1):134. doi:10.1186/s12943-017-0683-y
21. Wang C, Zhang Y, Dong Y. Lipid nanoparticle-mRNA formulations for therapeutic applications. *Acc Chem Res.* 2021;54(23):4283–4293. doi:10.1021/acs.accounts.1c00550
22. van der Meel R, Sulheim E, Shi Y, Kiessling F, Mulder WJM, Lammers T. Smart cancer nanomedicine. *Nat Nanotechnol.* 2019;14(11):1007–1017. doi:10.1038/s41565-019-0567-y
23. Riley RS, June CH, Langer R, Mitchell MJ. Delivery technologies for cancer immunotherapy. *Nat Rev Drug Discov.* 2019;18(3):175–196. doi:10.1038/s41573-018-0006-z
24. Liu Q, Das M, Liu Y, Huang L. Targeted drug delivery to melanoma. *Adv Drug Deliv Rev.* 2018;127:208–221. doi:10.1016/j.addr.2017.09.016
25. Sun T, Zhang YS, Pang B, Hyun DC, Yang M, Xia Y. Engineered nanoparticles for drug delivery in cancer therapy. *Angew Chem Int Ed Engl.* 2014;53(46):12320–12364. doi:10.1002/anie.201403036
26. Liu-Smith F, Dellinger R, Meyskens FL. Updates of reactive oxygen species in melanoma etiology and progression. *Arch Biochem Biophys.* 2014;563:51–55. doi:10.1016/j.abb.2014.04.007
27. Obrador E, Liu-Smith F, Dellinger RW, Salvador R, Meyskens FL, Estrela JM. Oxidative stress and antioxidants in the pathophysiology of malignant melanoma. *Biol Chem.* 2019;400(5):589–612. doi:10.1515/hsz-2018-0327
28. Wang Y, Yuan Q, Feng W, et al. Targeted delivery of antibiotics to the infected pulmonary tissues using ROS-responsive nanoparticles. *J Nanobiotechnology.* 2019;17(1):103. doi:10.1186/s12951-019-0537-4
29. Yin W, Ke W, Chen W, et al. Integrated block copolymer prodrug nanoparticles for combination of tumor oxidative stress amplification and ROS-responsive drug release. *Biomaterials.* 2019;195:63–74. doi:10.1016/j.biomaterials.2018.12.032
30. Liang J, Liu B. ROS-responsive drug delivery systems. *Bioeng Transl Med.* 2016;1(3):239–251. doi:10.1002/btm2.10014
31. Tang M, Hu P, Zheng Q, et al. Polymeric micelles with dual thermal and reactive oxygen species (ROS)-responsiveness for inflammatory cancer cell delivery. *J Nanobiotechnology.* 2017;15(1):39. doi:10.1186/s12951-017-0275-4
32. Zheng Q, Hu P, Tang Q, et al. Dually responsive amphiphilic block copolymer with oxidation-responsiveness and tuneable LCST behaviours. *Mater Lett.* 2017;201:133–136. doi:10.1016/j.matlet.2017.05.018
33. Napoli A, Valentini M, Tirelli N, Müller M, Hubbell JA. Oxidation-responsive polymeric vesicles. *Nat Mater.* 2004;3(3):183–189. doi:10.1038/nmat1081
34. Li L, Wang Y, Guo R, et al. Ginsenoside Rg3-loaded, reactive oxygen species-responsive polymeric nanoparticles for alleviating myocardial ischemia-reperfusion injury. *J Control Release.* 2020;317:259–272. doi:10.1016/j.jconrel.2019.11.032
35. Liu M, Liu S, Zhu X, et al. Tanshinone IIA-loaded micelles functionalized with rosmarinic acid: a novel synergistic anti-inflammatory strategy for treatment of atherosclerosis. *J Pharm Sci.* 2022;111(10):2827–2838. doi:10.1016/j.xphs.2022.05.007
36. Piskounova E, Agathocleous M, Murphy MM, et al. Oxidative stress inhibits distant metastasis by human melanoma cells. *Nature.* 2015;527(7577):186–191. doi:10.1038/nature15726

37. Nel AE, Mädler L, Velegol D, et al. Understanding biophysicochemical interactions at the nano-bio interface. *Nat Mater*. 2009;8(7):543–557. doi:10.1038/nmat2442
38. Verma A, Uzun O, Hu Y, et al. Surface-structure-regulated cell-membrane penetration by monolayer-protected nanoparticles. *Nat Mater*. 2008;7(7):588–595. doi:10.1038/nmat2202
39. Majumdar D, Jung KH, Zhang H, et al. Luteolin nanoparticle in chemoprevention: in vitro and in vivo anticancer activity. *Cancer Prev Res*. 2014;7(1). doi:10.1158/1940-6207.CAPR-13-0230
40. Wang Y, Wang Q, Feng W, et al. Folic acid-modified ROS-responsive nanoparticles encapsulating luteolin for targeted breast cancer treatment. *Drug Deliv*. 2021;28(1):1695–1708. doi:10.1080/10717544.2021.1963351
41. Qing W, Wang Y, Li H, Ma F, Zhu J, Liu X. Preparation and characterization of copolymer micelles for the solubilization and in vitro release of luteolin and luteoloside. *AAPS Pharm Sci Tech*. 2017;18(6):2095–2101. doi:10.1208/s12249-016-0692-y
42. Elsayed MMA, Okda TM, Atwa GMK, Omran GA, Abd Elbaky AE, Ramadan AEH. Design and optimization of orally administered luteolin nanoethosomes to enhance its anti-tumor activity against hepatocellular carcinoma. *Pharmaceutics*. 2021;13(5):648. doi:10.3390/pharmaceutics13050648
43. Shin K, Choi H, Song SK, et al. Nanoemulsion vehicles as carriers for follicular delivery of luteolin. *ACS Biomater Sci Eng*. 2018;4(5):1723–1729. doi:10.1021/acsbomaterials.8b00220
44. Fried L, Arbiser JL. The reactive oxygen-driven tumor: relevance to melanoma. *Pigment Cell Melanoma Res*. 2008;21(2):117–122. doi:10.1111/j.1755-148X.2008.00451.x
45. Cheung EC, Vousden KH. The role of ROS in tumour development and progression. *Nat Rev Cancer*. 2022;22(5):280–297. doi:10.1038/s41568-021-00435-0
46. Hayes JD, Dinkova-Kostova AT, Tew KD. Oxidative stress in cancer. *Cancer Cell*. 2020;38(2):167–197. doi:10.1016/j.ccell.2020.06.001
47. Napoli A, Tirelli N, Wehrli E, Hubbell JA. Lyotropic behavior in water of amphiphilic ABA triblock copolymers based on poly(propylene sulfide) and poly(ethylene glycol). *Langmuir*. 2002;18(22):8324–8329. doi:10.1021/la025897n
48. Velluto D, Demurtas D, Hubbell JA. PEG-b-PPS diblock copolymer aggregates for hydrophobic drug solubilization and release: cyclosporin A as an example. *Mol Pharm*. 2008;5(4):632–642. doi:10.1021/mp7001297
49. Gospodarowicz D, Delgado D, Vlodavsky I. Permissive effect of the extracellular matrix on cell proliferation in vitro. *Proc Natl Acad Sci USA*. 1980;77(7):4094–4098. doi:10.1073/pnas.77.7.4094
50. Pach E, Kümper M, Fromme JE, et al. Extracellular matrix remodeling by fibroblast-MMP14 regulates melanoma growth. *Int J Mol Sci*. 2021;22(22):12276. doi:10.3390/ijms222212276
51. Pautu V, Leonetti D, Lepeltier E, Clere N, Passirani C. Nanomedicine as a potent strategy in melanoma tumor microenvironment. *Pharmacol Res*. 2017;126:31–53. doi:10.1016/j.phrs.2017.02.014
52. Oglesby A, Algazi AP, Daud AI. Intratumoral and combination therapy in melanoma and other skin cancers. *Am J Clin Dermatol*. 2019;20(6):781–796. doi:10.1007/s40257-019-00452-8
53. Bommarreddy PK, Silk AW, Kaufman HL. Intratumoral approaches for the treatment of Melanoma. *Cancer J*. 2017;23(1):40–47. doi:10.1097/PPO.0000000000000234

Publish your work in this journal

The International Journal of Nanomedicine is an international, peer-reviewed journal focusing on the application of nanotechnology in diagnostics, therapeutics, and drug delivery systems throughout the biomedical field. This journal is indexed on PubMed Central, MedLine, CAS, SciSearch®, Current Contents®/Clinical Medicine, Journal Citation Reports/Science Edition, EMBase, Scopus and the Elsevier Bibliographic databases. The manuscript management system is completely online and includes a very quick and fair peer-review system, which is all easy to use. Visit <http://www.dovepress.com/testimonials.php> to read real quotes from published authors.

Submit your manuscript here: <https://www.dovepress.com/international-journal-of-nanomedicine-journal>